ADVANCED FUNCTIONAL MATERIALS
www.afm-journal.de

3D MoS_2–Graphene Microspheres Consisting of Multiple Nanospheres with Superior Sodium Ion Storage Properties

Seung Ho Choi, You Na Ko, Jung-Kul Lee, and Yun Chan Kang**

A novel anode material for sodium-ion batteries consisting of 3D graphene microspheres divided into several tens of uniform nanospheres coated with few-layered MoS_2 by a one-pot spray pyrolysis process is prepared. The first discharge/charge capacities of the composite microspheres are 797 and 573 mA h g^{-1} at a current density of 0.2 A g^{-1}. The 600th discharge capacity of the composite microspheres at a current density of 1.5 A g^{-1} is 322 mA h g^{-1}. The Coulombic efficiency during the 600 cycles is as high as 99.98%. The outstanding Na ion storage properties of the 3D MoS_2–graphene composite microspheres may be attributed to the reduced stacking of the MoS_2 layers and to the 3D structure of the porous graphene microspheres. The reduced stacking of the MoS_2 layers relaxes the strain and lowers the barrier for Na^+ insertion. The empty nanospheres of the graphene offer voids for volume expansion and pathways for fast electron transfer during repeated cycling.

1. Introduction

Rechargeable sodium-ion batteries have attracted much interest as a large-scale electrical energy storage system and specifically as an alternative to lithium-ion batteries owing to the abundance of sodium in nature.[1–7] Similar to the anode system of lithium batteries, on account of their higher theoretical specific capacities than carbon-based anode materials, metals, metal oxides, and metal sulfides have been extensively studied as promising anodes for rechargeable sodium-ion batteries.[8–26] Na^+ with its larger ionic radius and slower reaction kinetics than Li^+ causes large volume expansion and large polarization, resulting in low reversible capacities and poor cycle life.[4–6,27] Nanostructured Sn, Sb, SnSb, Fe_3O_4, CuO, and MoS_2 have been used to enhance the properties of rechargeable Na^+ batteries to overcome the inherent limitations of Na^+ systems.[13–26,28–30] However, reasonable design of electrode materials with high rate performance and long-cycle properties is still required for sodium-ion batteries.

S. H. Choi, Dr. Y. N. Ko, Prof. Y. C. Kang
Department of Materials Science and Engineering
Korea University
Anam-Dong, Seongbuk-Gu, Seoul 136-713,
Republic of Korea
E-mail: yckang@korea.ac.kr
Prof. J.-K. Lee
Department of Chemical Engineering
Konkuk University
1 Hwayang-Dong Gwangjin-Gu, Seoul 143-701, Republic of Korea
E-mail: jkrhee@konkuk.ac.kr

DOI: 10.1002/adfm.201402428

2D-layered metal dichalcogenides have been previously studied as electrode materials for rechargeable energy storage batteries.[28–45] Among metal dichalcogenides, layered MoS_2 has attracted much attention as a promising anode material. Graphene-like MoS_2 is covalently bonded to form 2D layers, which are stacked together through weak van der Waals interactions.[30] In lithium-ion batteries (LIBs), single and few-layer MoS_2 with various morphologies has been reported to facilitate fast Li^+ insertion/desertion process, resulting in an increase in the reversible capacity of MoS_2.[30,31] The WS_2 material with separated single- or few-layer sheets also showed excellent lithium ion storage properties.[32] Also, combinations with graphene materials have been regarded as fundamental strategies for enhancing the electrochemical properties of LIBs.[33–38] In light of this, 2D graphene sheets, owing to their excellent mechanical, thermal, and electrical properties, can be exploited as an ideal support for the graphene-like MoS_2.[31–38,42–45] Graphene sheets can restrict the stacking of MoS_2 and promote fast electron transport between the MoS_2 layer and the current collector.

The use of 3D graphene structures is more significant than 2D structures in energy storage system because 3D graphene structures with less aggregation maintain the superior intrinsic properties of graphene sheets, such as large surface area, novel physical properties, and structural stability.[46–49] Porous 3D graphene structure allows for easy electrolyte penetration and rapid Li^+ diffusion in lithium-ion batteries.[47–53] Also, 3D porous graphene sheets have been reported to mitigate volume changes during Li ion insertion and extraction by the absorption of stress, thereby improving the structural stability and cyclability of the electrode materials.[47–53] However, 3D graphene structures have been scarcely used in sodium-ion batteries.

In this study, we report the preparation of a novel structured-3D graphene microspheres divided into several tens of uniform nanospheres coated with few-layer MoS_2 layers by a one-pot spray pyrolysis process (Figure S1, Supporting Information). The nanospheres were surrounded by the few-layered graphene sheets, which were coated with MoS_2 layers. Further, we have applied these microspheres as an anode material for sodium-ion batteries. We expected the graphene nanospheres to accommodate the huge volume change of the MoS_2 layers during sodium ion insertion and extraction. Indeed, the novel structured MoS_2–graphene composite microspheres showed superior electrochemical properties as an anode material in

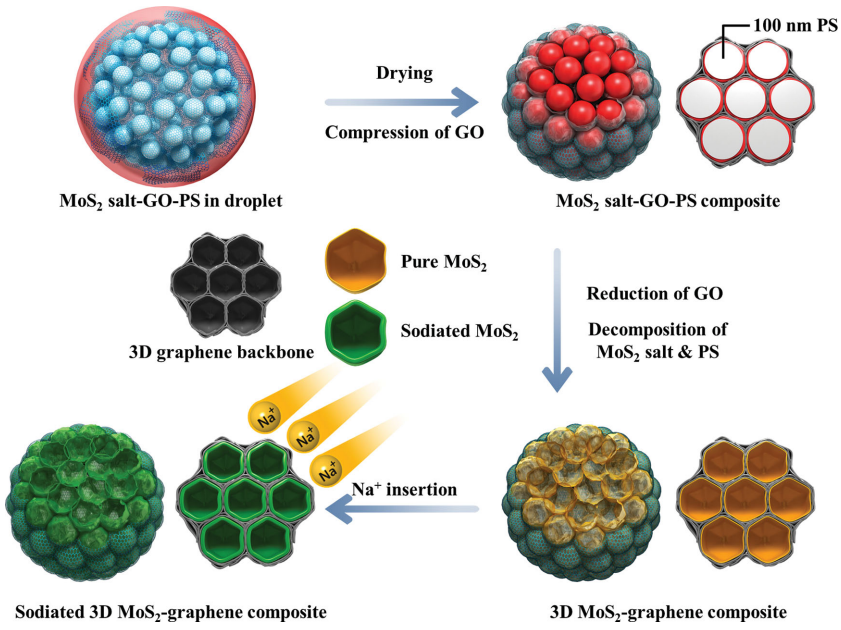

Scheme 1. Schematic diagram for the formation mechanism of the 3D MoS_2–graphene composite microsphere by the one-pot spray pyrolysis and description of Na^+ insertion process.

sodium-ion batteries in comparison to other materials reported in the literature.

2. Results and Discussion

3D MoS_2–graphene microspheres were directly prepared by ultrasonic spray pyrolysis from the colloidal solution of PS nanobeads, graphene oxide (GO), and $(NH_4)_2MoS_4$. PS nanobeads in the spray solution bonded to GO through hydrophobic interactions, and helped the dispersion of the GO sheets in the spray solution.[48,54] The MoS_4^{2-} ions formed by the dissolution of $(NH_4)_2MoS_4$ were not adsorbed on the surface of the negatively charged GO.[31,33] Therefore, a stable colloidal spray solution containing MoS_4^{2-} ions, GO sheets, and PS nanobeads could be obtained. Micrometer-sized droplets containing ammonium tetrathiomolybdate, GO, and PS nanobeads were formed by the ultrasonic nebulizer. The droplets, when passed through a tube furnace maintained at 800 °C, were transformed into MoS_2–graphene composite microspheres within a reaction time of 4 s. **Scheme 1** shows the mechanism of formation of the MoS_2–graphene composite microspheres by the one-pot spray pyrolysis. First, the drying of droplet produced a composite powder of ammonium tetrathiomolybdate, GO, and PS. Subsequently, the shrinking and compression of the GO sheets on the PS nanobeads during the evaporation of water (solvent) produced the embossed spherical microspheres. Ammonium tetrathiomolybdate was precipitated between the PS nanobeads and the GO layers. Thermal decompositions of the PS nanobeads and ammonium tetrathiomolybdate and the thermal reduction of GO into graphene resulted in the MoS_2–graphene composite microsphere. The thermal decomposition of the PS nanobeads into CO_2 and H_2O resulted in the formation of the empty nanospheres. The MoS_2–graphene layers covering the PS nanobeads formed the MoS_2-coated 3D graphene backbone composite structure. Consequently, 3D MoS_2–graphene composite microspheres consisting of multiple nanospheres of graphene coated with MoS_2 layers were prepared. As mentioned above, the PS nanobeads were applied to form the nanospheres. Therefore, the size of the graphene nanospheres could be easily controlled by changing the size of the PS nanobeads. In addition, the thicknesses of graphene backbone and MoS_2 layers could be controlled by changing the concentration of GO and the MoS_2 precursor in the spray solution.

Figure 1 shows the morphologies of the 3D MoS_2–graphene composite microspheres prepared by the one-pot spray pyrolysis described above. The field-emission scanning electron microscopy (FE-SEM) and transmission electron microscopy (TEM) images (as shown in Figure 1a–d) revealed the spherical 3D structure and uniform morphology. The average size of 3D MoS_2–graphene composite microspheres obtained from the FE-SEM image was 700 nm. The low-resolution TEM images, as shown in Figure 1c,d clearly indicate the empty multiple nanospheres present in the composite microspheres. The nanospheres were divided into thin backbone with layered structures, as shown by the high-resolution TEM images (Figure 1e,f). The enlarged TEM image (see Figure S2, Supporting Information) of the dotted circle portion in Figure 1e indicated clear lattice fringes separated by 0.27 nm, which corresponds to the interplanar distance between the (100) planes of layered MoS_2.[55] The coating layers observed in the enlarged TEM images shown in Figure S2 (Supporting Information) correspond to the MoS_2 layers coated over the graphene backbone, as shown in Scheme 1. The clear lattice fringes separated by 0.69 nm observed in the edge part shown by arrows in Figure 1f correspond to the (002) plane of the layered MoS_2.[31,33–35] The TEM images showed the average number of MoS_2 layers for 3D MoS_2–graphene composite to be 3–5 layers (see Figure 1e,f). The elemental mapping images shown in Figure 1g indicated the uniform distribution of Mo, S, and C all over the layered MoS_2–graphene composite microsphere. In addition, the high resolution elemental mapping images as shown in Figure S3 (Supporting Information) confirmed the void space of individual MoS_2–graphene nanospheres and uniform distribution of Mo, S, and C elements around the nanospheres. The graphene layers seem to act as the skeleton to enable the formation of 3D MoS_2–graphene composite microspheres. The graphene layers also minimized the stacking of the layered MoS_2 during the formation of the composite microspheres.

Figure 2 shows the morphologies of the MoS_2–graphene composite microspheres prepared from the spray solution without the PS nanobeads. The composite powders showed crumpled and irregular structures, as demonstrated by the FE-SEM and TEM images shown in Figure 2a–d. The high-resolution TEM images shown in Figure 2e,f indicate the presence of highly stacked MoS_2 layers. The elemental mapping

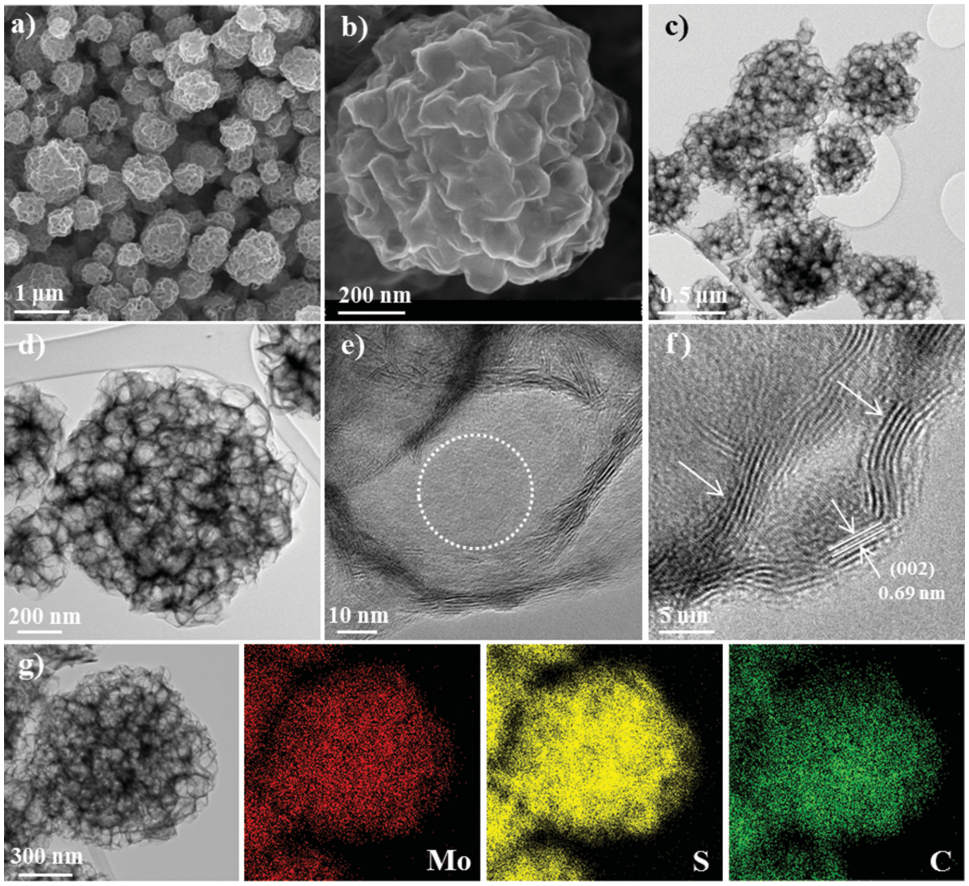

Figure 1. Morphologies of the 3D MoS_2–graphene composite microspheres. a,b) FE-SEM images; c–f) TEM images; g) elemental mapping images of Mo, S, and C components.

images shown in Figure 2g reveals the uniform distribution of Mo, S, and C all over the crumpled MoS_2–graphene composite powder. The selected area electron diffraction (SAED) patterns as shown in Figure S4 (Supporting Information) are indicative of the polycrystalline structures of the MoS_2–graphene composites prepared by spray pyrolysis.

Figure 3a shows the X-ray diffractometry (XRD) patterns of the MoS_2–graphene composite materials prepared by one-pot spray pyrolysis from spray solutions with and without PS nanobeads. Both samples were polycrystalline containing hexagonal MoS_2 (JCPDS 37–1492).[37,38] The weak (002) peak of the 3D MoS_2–graphene composite microsphere demonstrated the presence of "graphene-like" MoS_2 layers (i.e., less than five layers).[30,33,39] In the synthesis step, PS nanobeads, which functioned as templates, minimized the phase separation and stacking of the MoS_2 layers. The oxidation state and composition of the 3D MoS_2–graphene composite microspheres were analyzed by X-ray photoelectron spectroscopy (XPS) (see Figure 3b). The XPS profile of the MoS_2–graphene composite microspheres indicated two strong peaks at around 229.4 and 232.5 eV, which can be attributed to Mo3$d_{5/2}$ and Mo3$d_{3/2}$ binding energies of MoS_2, respectively, while the peak at 226.6 eV can be indexed as S2s.[56,57] The peaks at 162.0 and 163.1 eV shown in Figure S5 (Supporting Information) can be indexed to the S2$p_{3/2}$ and S2$p_{1/2}$ binding energies of MoS_2, respectively.[56,57] The S/Mo atomic ratio was measured as 2.3 by XPS analysis. The results of the XPS and XRD analyses were consistent with the reported values for few layered MoS_{2+x} crystals.[30,33] The C1s XPS profile of the MoS_2–graphene composite microspheres, as shown in Figure 3c, showed a strong peak corresponding to sp^2 C–C bonds at 284.6 eV.[58] In general, the C1s spectrum of GO showed two main peaks centered at 284.6 and 286.7 eV, which correspond to the binding energy of the sp^2 C–C bonds and C–O bonds, respectively.[58] Therefore, the C1s spectrum of the MoS_2–graphene composite microspheres indicated the complete reduction of GO (with oxygen containing functionalized groups) into graphene in the reactor maintained at 800 °C. Considering that MoS_2 is converted into MoO_3 when heated in air, the graphene content in the MoS_2–graphene composite microspheres was 16.4 wt%, as measured by thermogravimetric analysis (see Figure S6, Supporting Information). The Barrett–Joyner–Halenda pore size distributions of both samples are shown in Figure 3d. The 3D MoS_2–graphene composite microspheres contained more well-developed mesopores than did the crumpled MoS_2–graphene composite powders. The Brunauer–Emmett–Teller (BET) surface areas of the MoS_2–graphene composite materials prepared from the spray solutions with and without PS nanobeads were 33 and 10 $m^2\ g^{-1}$, respectively.

The electrochemical properties of the 3D MoS_2–graphene composite microspheres and crumpled MoS_2–graphene

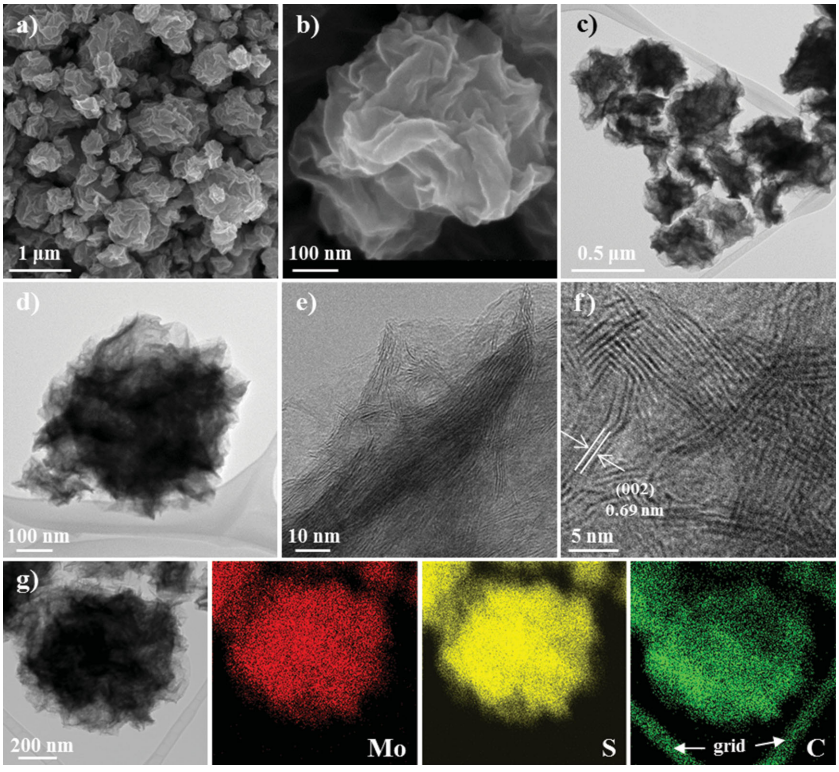

Figure 2. Morphologies of the crumpled MoS_2–graphene composite microspheres. a,b) FE-SEM images; c–f) TEM images; g) elemental mapping images of Mo, S, and C components.

composite powders are shown in **Figure 4**. Figure 4a shows the cyclic voltammograms (CVs) of the 3D MoS_2–graphene composite microspheres for the first three cycles at a scan rate of 0.1 mV s^{-1} at voltages in the range 0.001–3 V. The reduction of MoS_2 in a Na-ion battery can be described by the equation $MoS_2 + 4Na^+ + 4e^- \rightarrow Mo + 2Na_2S$.[28–30] In the first cathodic scan, peaks ranging from 0.5 to 3.0 V are associated with Na^+ insertion between the MoS_2 and graphene layers and the formation of the solid electrolyte interface (SEI) layer owing to the decomposition of the electrolyte.[21–23,29,59] The peak under 0.5 V in the deep cathodic process could be assigned to the electrochemical decomposition of MoS_2 to form metallic (Mo) nanograins embedded in an amorphous Na_2S matrix.[29,30] A broad oxidation peak was observed at 1.7 V in the first charging process, which corresponded to the oxidation of the Mo nanograins to MoS_2.[29,30] Beyond the first cycle, the reduction peak at 0.1 V disappeared and the second and third discharging/charging curves almost overlapped, suggesting high reversibility and cycling stability of Na^+ storage in the 3D MoS_2–graphene composite microspheres.

Figure 4b shows the 1st, 2nd, and 50th charge–discharge curves of the two samples at a constant current density of 0.2 A g^{-1}. The initial discharge curves of the 3D MoS_2–graphene composite microspheres and crumpled MoS_2–graphene composite powders consisted of slight plateaus near 1.1 and 0.8 V, respectively. The potential plateaus seen in the first discharge curves of the two samples were replaced by long slopes between 2.5 and 0.001 V from the second cycle onwards. During the first charging process, the distorted MoS_2 structure failed to fully recover to the pristine MoS_2 structure. The initial discharge and charge capacities of the 3D MoS_2–graphene composite microspheres were 797 and 573 mA h g^{-1}, respectively, and the corresponding initial Coulombic efficiency was 72%. However, the initial discharge and charge capacities of the crumpled MoS_2–graphene composite powders were 415 and 511 mA h g^{-1}, respectively, and the corresponding initial Coulombic efficiency was 81%. Reduced GO shows a large irreversible capacity in the first cycle, which originates from the formation of the SEI layer on the electrode surface and from the reaction of the sodium ions with residual oxygen-containing functional groups.[60] The high surface area and large pore volume also resulted in a low initial Coulombic efficiency for the 3D MoS_2–graphene composite microspheres. The 50th reversible discharge capacities of the 3D MoS_2–graphene composite microspheres and crumpled MoS_2–graphene composite powders, as shown in Figure 4c, were 480 and 320 mA h g^{-1}, respectively, and the corresponding capacity retentions measured after the first cycles were 88% and 83%. The rate capabilities of the two samples were evaluated at high current densities ranging from 1 to 10 A g^{-1} and then at 1 A g^{-1}, as shown in Figure 4d. The charge and discharge curves for rate performances were shown in Figure S7 (Supporting Information). The average discharge capacities of the 3D MoS_2–graphene composite microspheres were 427, 355, 306, 273, and 234 mA h g^{-1} when cycled at current densities of 1, 3, 5, 7, and 10 A g^{-1}, respectively. The crumpled MoS_2–graphene composite powders showed average discharge capacities of 311, 232, 178, 136, and 80 mA h g^{-1} when cycled at current densities of 1, 3, 5, 7, and 10 A g^{-1}, respectively. The rate retentions of the 3D MoS_2–graphene composite microspheres and crumpled MoS_2–graphene composite powders were 55% and 26%, when the current density increased from 1 to 10 A g^{-1}. The decreased Na^+ diffusion distance and enhanced electrical connectivity resulted in the superior rate performance of the 3D MoS_2–graphene composite microspheres. The rate capabilities of the two samples were evaluated at low current densities ranging between 0.1 and 0.9 A g^{-1}, and then at 0.1 A g^{-1}, as shown in Figure S8 (Supporting Information). The average discharge capacities of the 3D MoS_2–graphene composite microspheres were 535 and 412 mA h g^{-1} when cycled at 0.1 and 0.9 A g^{-1}, respectively. The crumpled MoS_2–graphene composite powders showed average discharge capacities of 380 and 283 mA h g^{-1} when cycled at 0.1 and 0.9 A g^{-1}, respectively. The rate retentions of the 3D MoS_2–graphene composite microspheres and crumpled MoS_2–graphene composite powders showed similar values of 77% and 74% when the current density was increased from 0.1 to 0.9 A g^{-1}. Additionally, after the rate test, the discharge capacities and Coulombic efficiencies of the 3D MoS_2–graphene composite microspheres during an additional 600 cycles were measured at a higher rate of

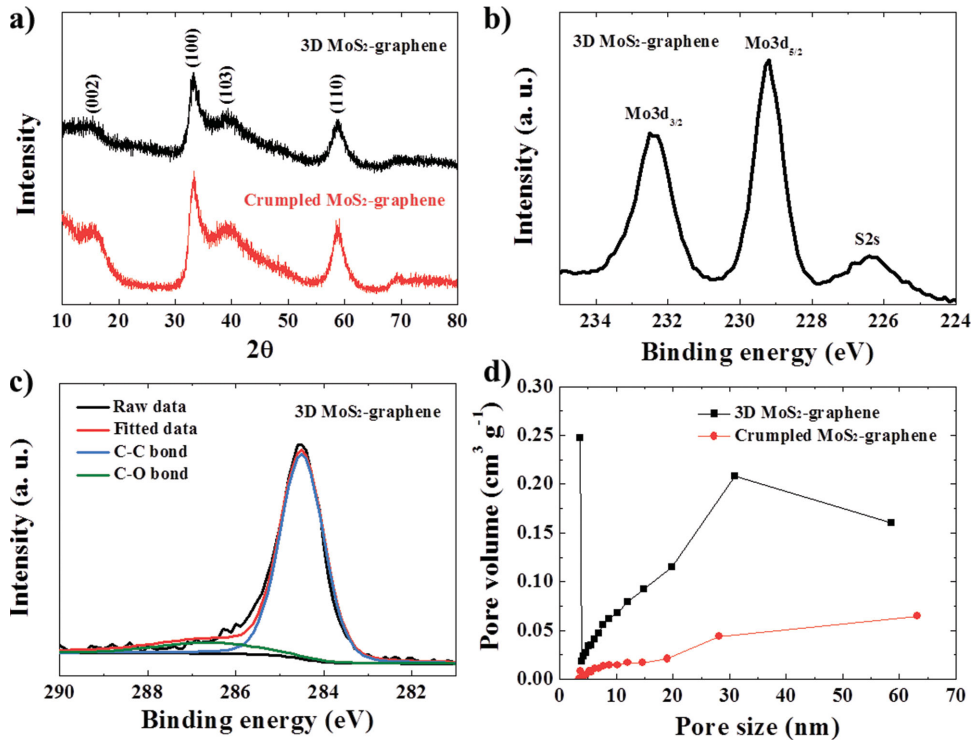

Figure 3. Properties of the 3D MoS_2–graphene composite and the crumpled MoS_2–graphene composite microspheres. a) XRD patterns; b) XPS spectrum of Mo3*d* of the 3D MoS_2–graphene composite microspheres; c) XPS spectrum of C1s of the 3D MoS_2–graphene composite microspheres; and d) pore size distributions.

1.5 A g^{-1} for a long period cycle test (see Figures 4e and S7, Supporting Information). The first and 600th discharge capacities of the 3D MoS_2–graphene composite microspheres at a current density of 1.5 A g^{-1} were 385 and 322 mA h g^{-1}, respectively, and the corresponding capacity retention was 84%. The average Coulombic efficiency during the additional 600 cycles was as high as 99.98%. In general, achieving fast and stable Na^+ storage properties in sodium-ion batteries is challenging because of large ionic radius of Na^+. The outstanding electrochemical properties of the 3D MoS_2–graphene composite microspheres are related to the reduced stacking of the MoS_2 layers and the 3D porous graphene microspheres. The low stacking of the MoS_2 layers relaxed the strain and lowered the barrier for Na^+ insertion.[30,31] The empty nanospheres of graphene offered sufficient void spaces for volume expansion and fast electron transfer pathways during repeated cycling. The morphologies of the 3D MoS_2–graphene composite microsphere obtained after first Na^+ insertion and desertion processes are shown in Figures S9–S11 (Supporting Information). The lattice fringes of MoS_2 nanocrystals were not observed from the TEM image of the microsphere obtained after 1st discharging process as shown in Figure S10b (Supporting Information). The TEM and elemental mapping images shown in Figure S10c (Supporting Information) revealed the inserted Na component in the composite microsphere during the 1st discharging process. The composite microspheres obtained after 1st discharging and charging processes had similar sizes and morphologies. **Figure 5** shows the TEM and elemental mapping images and SAED pattern of the 3D MoS_2–graphene composite microspheres obtained after 50 cycles at a current density of 0.2 A g^{-1}. The 3D graphene nanospheres of the 3D graphene-MoS_2 composite microsphere were maintained, as shown in the TEM images (see Figure 5a,b). The SAED ring pattern with a faint ring diffraction spot indicates the amorphous-like structure of the 3D MoS_2–graphene composite microspheres subjected to 50 cycles, as shown in Figure 5c. Mo and S were uniformly dispersed all over the graphene microsphere without aggregation even after 50 cycles, as shown in the elemental mapping images (see Figure 5d). The empty nanosphere provided sufficient void space for the large volume expansion of MoS_2 during the Na^+ insertion process.

To understand why the 3D MoS_2–graphene composite microspheres exhibited superior electrochemical performances compared with the crumpled MoS_2–graphene composite powders, impedance measurements were carried out before cycling and after 50 cycles at a constant current density of 0.2 A g^{-1}, as shown **Figure 6**. The medium frequency semicircle is attributed to the charge-transfer resistance (R_{ct}) between the active material and the electrolyte, and the low frequency region corresponds to the sodium diffusion process within the electrodes.[61–64] The charge-transfer resistances of the 3D MoS_2–graphene composite microspheres and crumpled MoS_2–graphene composite powders were 250 and 374 Ω before cycling, respectively, and the corresponding values were 35 and 56 Ω after the 50th cycle, as shown in Figure 6a,b. Figure 6c,d shows the relationship between Z_{re} and $\omega^{-1/2}$ in the low frequency region, where ω is the angular frequency in the low frequency region ($\omega = 2\pi f$). The low slope at low frequency indicates good

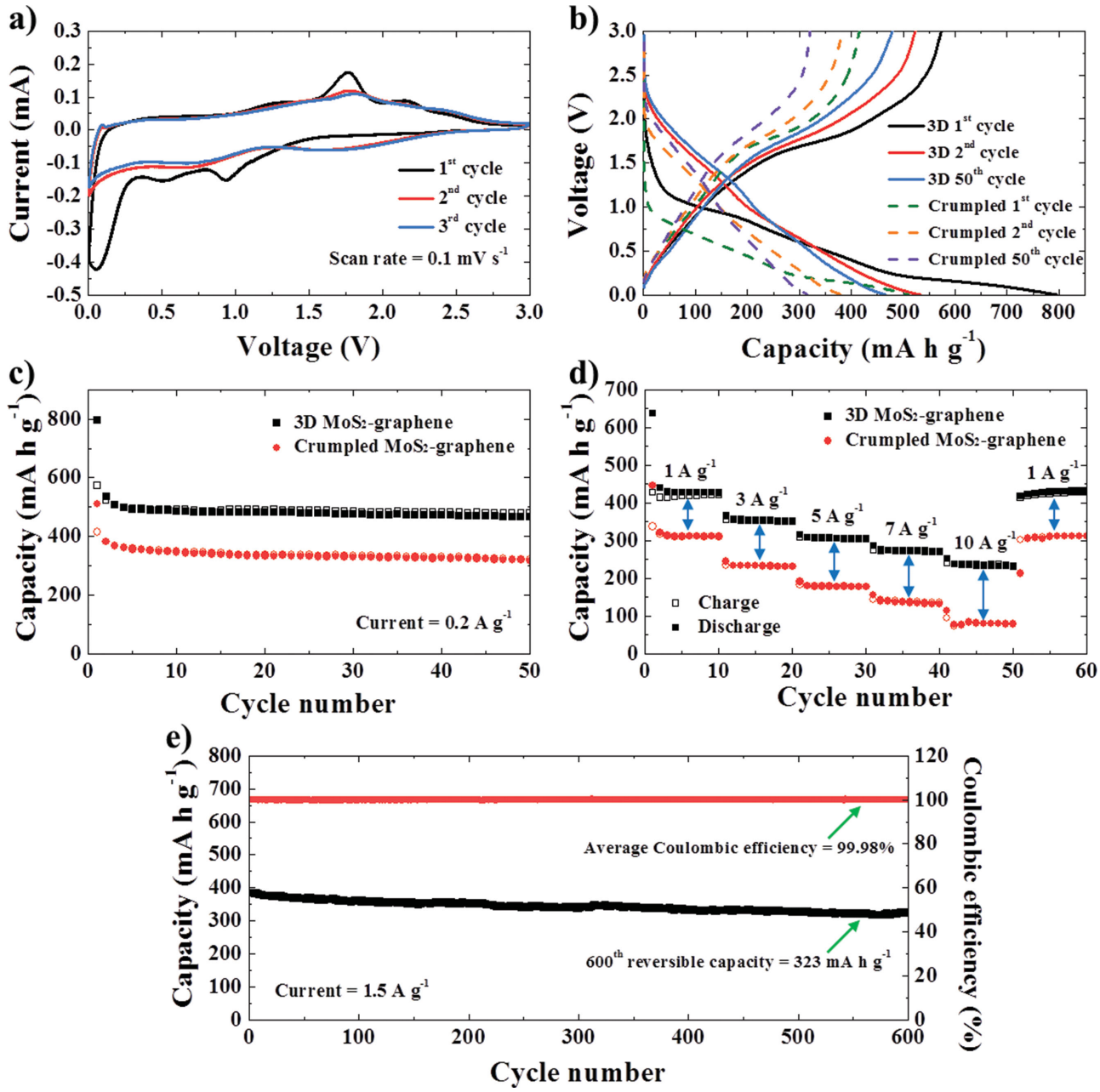

Figure 4. Electrochemical properties of the 3D MoS_2–graphene composite and the crumpled MoS_2–graphene composite microspheres. a) CV curves of the 3D MoS_2–graphene composite microspheres; b) charge/discharge curves at a current density of 0.2 A g^{-1}; c) cycling performances at a current density of 0.2 A g^{-1}; d) high rate performances; and e) long-term cycling properties and Coulombic efficiencies of the 3D MoS_2–graphene composite microspheres at a current density of 1.5 A g^{-1}.

sodium ion kinetics in the electrode materials.[61–64] The 3D MoS_2–graphene composite microspheres showed lower slopes than the crumpled MoS_2–graphene composite powders before cycling and after 50th cycle, as shown in Figure 6c,d. The 3D MoS_2–graphene composite microspheres showed smaller charge transfer resistance and better Na^+ kinetics than the crumpled MoS_2–graphene composite powders.

The Na^+ storage properties of the 3D MoS_2–graphene composite microspheres were compared with those of MoS_2 electrodes of various morphologies reported previously in the literature. Composite layered paper consisting of acid-exfoliated MoS_2 nanoflakes in a reduced GO matrix has been reported to show a stable charge capacity of approximately 230 mA h g^{-1} after 20 cycles at a current density of 0.025 A g^{-1}.[29] The single layered ultrasmall nanoplates of MoS_2 embedded in thin carbon nanowires exhibited a high discharge capacity of 321 mA h g^{-1} after 100 cycles at a current density of 1.0 A g^{-1} and the corresponding discharge

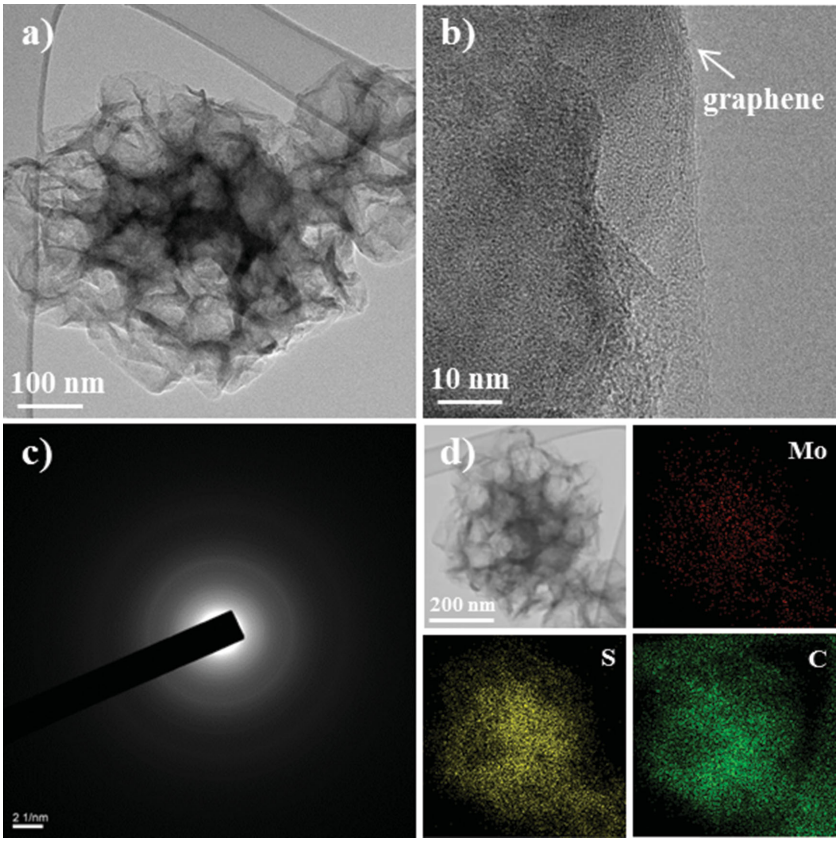

Figure 5. TEM images and SAED pattern of the 3D MoS_2–graphene composite microspheres after 50th cycle at a current density of 0.2 A g^{-1}. a,b) TEM images; c) SAED pattern; d) elemental mapping images of Mo, S, and C components.

capacity retention measured after the first cycle was 60%.[30] However, the discharge capacity of the MoS_2–graphene composite microspheres after 600 cycles at a current density of 1.5 A g^{-1} was as high as 322 mA h g^{-1}.

3. Conclusion

In summary, the 3D MoS_2–graphene composite microspheres with superior Na^+ storage properties were prepared by a one-pot spray pyrolysis process. The 3D MoS_2–graphene composite microspheres consisted of multiple nanospheres of graphene coated with MoS_2 layers. The size of the graphene nanospheres could be easily controlled by changing the size of the PS nanobead templates used in the spray solution. In addition, the thicknesses of the graphene sheets and MoS_2 layers could be controlled by changing the concentration of GO and MoS_2 precursor in the spray solution. The 3D MoS_2–graphene composite microspheres showed superior Na^+ storage capacities than the crumpled MoS_2–graphene composite powders prepared under identical conditions (albeit without the PS bead templates). Our study indicates that the novel 3D graphene-MoS_2 composite microspheres can be successfully applied as a high potential anode material in sodium-ion batteries. The 3D MoS_2–graphene composite microspheres showed outstanding Na^+ storage properties for high capacity, fast charge/discharge, and long cycle life due to synergy effect of the reduced stacking of the MoS_2 layers and the 3D structure of the porous graphene microspheres. The simple process introduced in this study could be also widened to the preparation of 3D metal sulfide-graphene composite microspheres with various compositions for a wider range of applications.

4. Experimental Section

Preparation of 3D MoS_2-Graphene Composite Microspheres: Graphene oxide (GO) was synthesized using a modified Hummer's method from graphite nanoflakes.[53] 3D MoS_2–graphene microspheres were directly prepared by ultrasonic spray pyrolysis at 800 °C. A quartz reactor with a length of 1200 and diameter of 50 mm was used for the synthesis, along with a nitrogen (carrier gas) flow rate of 5 L min^{-1}. The as-obtained GO was redispersed in distilled water and exfoliated by ultrasonication to generate the GO sheets. Ammonium tetrathiomolybdate ($(NH_4)_2MoS_4$, Aldrich, 1.63 g) was dissolved in 500 mL of the exfoliated GO solution (1 mg ml^{-1}). Then, 4.5 g of polystyrene (PS) nanobeads with a diameter of 100 nm were added into the GO sheet-ammonium tetrathiomolybdate solution.

Characterization: The crystal structures of the prepared samples were investigated by X-ray diffractometry (XRD, X'pert PRO MPD) using Cu K_α radiation (λ = 1.5418 Å). The morphological features of the samples were investigated using field-emission scanning electron microscopy (FE-SEM, S-4800) and high-resolution transmission electron microscopy (HR-TEM, JEM-2100F) at a working voltage of 200 kV. The specific surface areas of the prepared samples were calculated by the Brunauer–Emmett–Teller (BET) analysis of the nitrogen adsorption measurements (TriStar 3000). The samples were also investigated using X-ray photoelectron spectroscopy (XPS, ESCALAB-210) with Al Kα radiation (1486.6 eV).

Electrochemical Measurements: The capacities and cycling properties of the prepared samples were determined by fabricating 2032-type coin cells. The electrode contained a mixture of 70 wt% of the active material, 15 wt% of Super P, and 15 wt% of sodium carboxymethyl cellulose (CMC) binder. Stick-type sodium metal and microporous polypropylene film were used as the counter electrode and separator, respectively. The electrolyte was a solution of 1 M $NaClO_4$ (Aldrich) in a 1:1 volume mixture of ethylene carbonate/dimethyl carbonate (EC/DMC) to which 5 wt% fluoroethylene carbonate was added. The charge–discharge characteristics of the samples were determined by cycling in the potential range 0.001–3.0 V at fixed current densities. Cyclic voltammetry (CV) was carried out at a scan rate of 0.1 mV s^{-1}. The dimensions of the negative electrode were 1 cm × 1 cm and the mass loading was approximately 1.2 mg cm^{-2}. The capacities described in this study were based on the total weight of 3D MoS_2–graphene composite. Electrochemical impedance spectroscopy (EIS) of the electrode was measured over a frequency range of 0.01 Hz–100 kHz.

Supporting Information

Supporting Information is available from the Wiley Online Library or from the author.

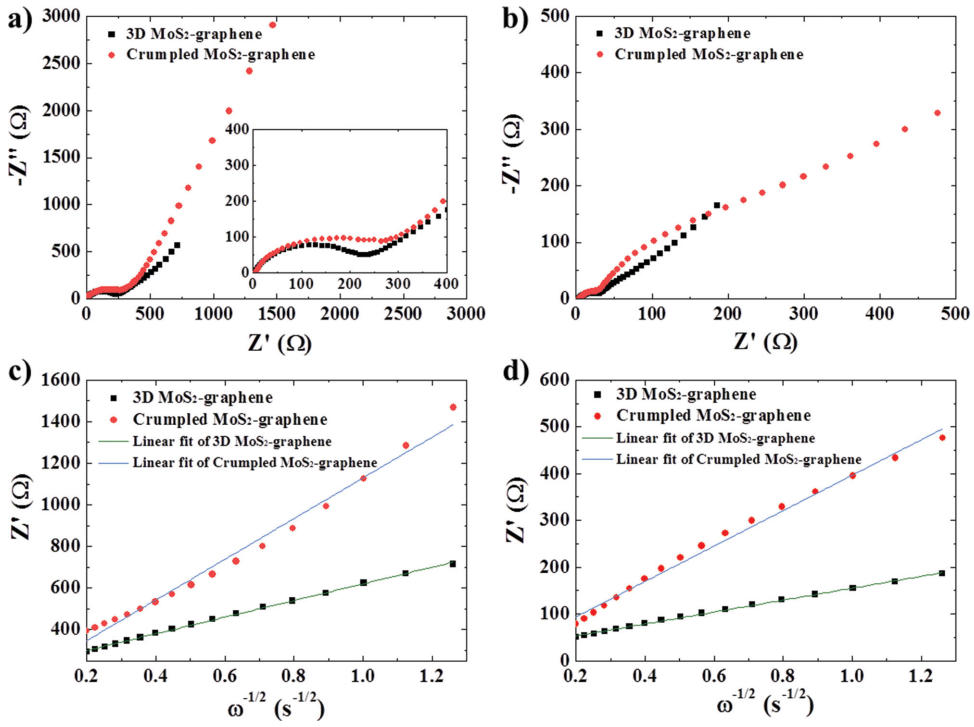

Figure 6. Electrochemical impedance spectroscopy (EIS) and relationship between Z′ and $\omega^{-1/2}$ in the low-frequency region of the 3D MoS_2–graphene composite and the crumpled MoS_2–graphene composite microspheres. a,b) EIS spectra before cycling and after 50th cycle. c,d) Linear fits in the low-frequency region before cycling and after 50th cycle.

Acknowledgements

This work was supported by the National Research Foundation of Korea (NRF) grant funded by the Korean Government (MEST) (Grant No. 2012R1A2A2A02046367). This work was supported by the Energy Efficiency & Resources Core Technology Program of the Korea Institute of Energy Technology Evaluation and Planning (KETEP), granted financial resource from the Ministry of Trade, Industry & Energy, Republic of Korea (201320200000420).
Note: The first affiliation was missing the name Korea University in the initial online version. This was corrected as a part of the issue on March 25, 2015.

Received: July 21, 2014
Revised: January 12, 2015
Published online: February 3, 2015

[1] B. Dunn, H. Kamath, J. M. Tarascon, *Science* **2011**, *334*, 928.
[2] S. W. Kim, D. H. Seo, X. Ma, G. Ceder, K. Kang, *Adv. Energy Mater.* **2012**, *2*, 710.
[3] M. D. Slater, D. Kim, E. Lee, C. S. Johnson, *Adv. Funct. Mater.* **2013**, *23*, 947.
[4] H. Pan, Y. S. Hu, L. Chen, *Energy Environ. Sci.* **2013**, *6*, 2338.
[5] B. L. Ellis, L. F. Nazar, *Curr. Opin. Solid State Mater. Sci.* **2012**, *16*, 168.
[6] V. Palomares, P. Serras, I. Villaluenga, K. B. Hueso, J. Carretero-González, T. Rojo, *Energy Environ. Sci.* **2012**, *5*, 5884.
[7] E. M. Lotfabad, J. Ding, K. Cui, A. Kohandehghan, W. P. Kalisvaart, M. Hazelton, D. Mitlin, *ACS Nano* **2014**, *8*, 7115.
[8] M. V. Reddy, G. V. S. Rao, B. V. R. Chowdari, *Chem. Rev.* **2013**, *113*, 5364.
[9] N. S. Choi, Z. Chen, S. A. Freunberger, X. Ji, Y. K. Sun, K. Amine, G. Yushin, L. F. Nazar, J. Cho, P. G. Bruce, *Angew. Chem. Inter. Ed.* **2012**, *51*, 9994.
[10] J. Jiang, Y. Li, J. Liu, X. Huang, C. Yuan, X. W. Lou, *Adv. Mater.* **2012**, *24*, 5166.
[11] F. Cheng, J. Liang, Z. Tao, J. Chen, *Adv. Mater.* **2011**, *23*, 1695.
[12] H. Zhang, L. Zhou, O. Noonan, D. J. Martin, A. K. Whittaker, C. Yu, *Adv. Funct. Mater.* **2014**, *24*, 4337.
[13] Y. Xu, Y. Zhu, Y. Liu, C. Wang, *Adv. Energy Mater.* **2013**, *3*, 128.
[14] L. Ji, M. Gu, Y. Shao, X. Li, M. H. Engelhard, B. W. Arey, W. Wang, Z. Nie, J. Xiao, C. Wang, J. G. Zhang, J. Liu, *Adv. Mater.* **2014**, *26*, 2901.
[15] M. He, K. Kravchyk, M. Walter, M. V. Kovalenko, *Nano Lett.* **2014**, *14*, 1255.
[16] Y. Zhu, X. Han, Y. Xu, Y. Liu, S. Zheng, K. Xu, L. Hu, C. Wang, *ACS Nano* **2013**, *7*, 6378.
[17] S. Komaba, W. Murata, T. Ishikawa, N. Yabuuchi, T. Ozeki, T. Nakayama, A. Ogata, K. Gotoh, K. Fujiwara, *Adv. Funct. Mater.* **2011**, *21*, 3859.
[18] S. Yuan, X. L. Huang, D. L. Ma, H. G. Wang, F. Z. Meng, X. B. Zhang, *Adv. Mater.* **2014**, *26*, 2273.
[19] Z. Jian, B. Zhao, P. Liu, F. Li, M. Zheng, M. Chen, Y. Shi, H. Zhou, *Chem. Commun.* **2014**, *50*, 1215.
[20] S. M. Oh, S. T. Myung, C. S. Yoon, J. Lu, J. Hassoun, B. Scrosati, K. Amine, Y. K. Sun, *Nano Lett.* **2014**, *14*, 1620.
[21] L. Wang, K. Zhang, Z. Hu, W. Duan, F. Cheng, J. Chen, *Nano Res.* **2014**, *7*, 199.
[22] Y. Xu, E. M. Lotfabad, H. Wang, B. Farbod, Z. Xu, A. Kohandehghan, D. Mitlin, *Chem. Commun.* **2013**, *49*, 8973.
[23] W. H. Ryu, J. W. Jung, K. Park, S. J. Kim, I. D. Kim, *Nanoscale* **2014**, *6*, 10975.
[24] D. Y. W. Yu, P. V. Prikhodchenko, C. W. Mason, S. K. Batabyal, J. Gun, S. Sladkevich, A. G. Medvedev, O. Lev, *Nat. Commun.* **2013**, *4*, 2922.

[25] B. Qu, C. Ma, G. Ji, C. Xu, J. Xu, Y. S. Meng, T. Wang, J. Y. Lee, *Adv. Mater.* **2014**, *26*, 3854.
[26] D. Su, S. Dou, G. Wang, *Chem. Commun.* **2014**, *50*, 4192.
[27] S. P. Ong, V. L. Chevrier, G. Hautier, A. Jain, C. Moore, S. Kim, X. Ma, G. Ceder, *Energy Environ. Sci.* **2011**, *4*, 3680.
[28] J. Park, J. S. Kim, J. W. Park, T. H. Nam, K. W. Kim, J. H. Ahn, G. Wang, H. J. Ahn, *Electrochim. Acta* **2013**, *92*, 427.
[29] L. David, R. Bhandavat, G. Singh, *ACS Nano* **2014**, *8*, 1759.
[30] C. Zhu, X. Mu, P. A. Aken, Y. Yu, J. Maier, *Angew. Chem. Int. Ed.* **2014**, *53*, 2152.
[31] Z. Wang, T. Chen, W. Chen, K. Chang, L. Ma, G. Huang, D. Chen, J. Y. Lee, *J. Mater. Chem. A* **2013**, *1*, 2202.
[32] R. Bhandavat, L. David, G. Singh, *J. Phys. Chem. Lett.* **2012**, *3*, 1523.
[33] K. Chang, D. Geng, X. Li, J. Yang, Y. Tang, M. Cai, R. Li, X. Sun, *Adv. Energy Mater.* **2013**, *3*, 839.
[34] K. Chang, W. Chen, *ACS Nano* **2011**, *5*, 4720.
[35] G. Huang, T. Chen, W. Chen, Z. Wang, K. Chang, L. Ma, F. Huang, D. Chen, J. Y. Lee, *Small* **2013**, *9*, 3693.
[36] X. Cao, Y. Shi, W. Shi, X. Rui, Q. Yan, J. Kong, H. Zhang, *Small* **2013**, *9*, 3433.
[37] H. Liu, D. Su, R. Zhou, B. Sun, G. Wang, S. Z. Qiao, *Adv. Energy Mater.* **2012**, *2*, 970.
[38] Y. Gong, S. Yang, L. Zhan, L. Ma, R. Vajtai, P. M. Ajayan, *Adv. Funct. Mater.* **2014**, *24*, 125.
[39] H. Hwang, H. Kim, J. Cho, *Nano Lett.* **2011**, *11*, 4826.
[40] S. Ding, D. Zhang, J. S. Chen, X. W. Lou, *Nanoscale* **2012**, *4*, 95.
[41] M. R. Gao, Y. F. Xu, J. Jiang, S. H. Yu, *Chem. Soc. Rev.* **2013**, *42*, 2986.
[42] M. Chhowalla, H. S. Shin, G. Eda, L. J. Li, K. P. Loh, H. Zhang, *Nat. Chem.* **2013**, *5*, 263.
[43] X. Huang, Z. Zeng, H. Zhang, *Chem. Soc. Rev.* **2013**, *42*, 1934.
[44] H. Wang, H. Feng, J. Li, *Small* **2014**, *10*, 2165.
[45] X. Huang, C. Tan, Z. Yin, H. Zhang, *Adv. Mater.* **2014**, *26*, 2185.
[46] Y. Chen, F. Guo, A. Jachak, S.-P. Kim, D. Datta, J. Liu, I. Kulaots, C. Vaslet, H. D. Jang, J. Huang, A. Kane, V. B. Shenoy, R. H. Hurt, *Nano Lett.* **2012**, *12*, 1996.
[47] Z. Chen, W. Ren, L. Gao, B. Liu, S. Pei, H. M. Cheng, *Nat. Mater.* **2011**, *10*, 424.
[48] B. G. Choi, M. H. Yang, W. H. Hong, J. W. Choi, Y. S. Huh, *ACS Nano* **2012**, *6*, 4020.
[49] J. Luo, J. Kim, J. Huang, *Acc. Chem. Res.* **2013**, *46*, 2225.
[50] C. Li, G. Shi, *Nanoscale* **2012**, *4*, 5549.
[51] X. Cao, B. Zheng, X. Rui, W. Shi, Q. Yan, H. Zhang, *Angew. Chem. Int. Ed.* **2014**, *53*, 1404.
[52] Y. Huang, D. Wu, J. Wang, S. Han, L. Lv, F. Zhang, X. Feng, *Small* **2014**, *10*, 2226.
[53] S. H. Choi, Y. C. Kang, *ChemSusChem* **2014**, *7*, 523.
[54] T. Y. Zhang, X. Q. Li, S. Z. Kang, L. X. Qin, W. F. Yan, J. Mua, *J. Colloid Interface Sci.* **2013**, *402*, 279.
[55] K. K. Liu, W. Zhang, Y. H. Lee, Y. C. Lin, M. T. Chang, C. Y. Su, C. S. Chang, H. Li, Y. Shi, H. Zhang, C. S. Lai, L. J. Li, *Nano Lett.* **2012**, *12*, 1538.
[56] Q. Wang, J. Li, *J. Phys. Chem. C* **2007**, *111*, 1675.
[57] Y. N. Ko, Y. C. Kang, S. B. Park, *Nanoscale* **2014**, *6*, 4508.
[58] H. A. Becerril, J. Mao, Z. Liu, R. M. Stoltenberg, Z. Bao, Y. Chen, *ACS Nano* **2008**, *2*, 463.
[59] X. Wang, X. Shen, Z. Wang, R. Yu, L. Chen, *ACS Nano* **2014**, *8*, 11394.
[60] Y. X. Wang, S. L. Chou, H. K. Liu, S. X. Dou, *Carbon* **2013**, *57*, 202.
[61] Y. Zhu, Y. Xu, Y. Liu, C. Luo, C. Wang, *Nanoscale* **2013**, *5*, 780.
[62] R. Ruffo, R. Fathi, D. J. Kim, Y. H. Jung, C. M. Mari, D. K. Kim, *Electrochim. Acta* **2013**, *108*, 575.
[63] Y. N. Ko, S. B. Park, K. Y. Jung, Y. C. Kang, *Nano Lett.* **2013**, *13*, 5462.
[64] Y. Shi, J. Z. Wang, S. L. Chou, D. Wexler, H. J. Li, K. Ozawa, H. K. Liu, Y. P. Wu, *Nano Lett.* **2013**, *13*, 4715.